

This document contains a post-print version of the paper:

“Time-Varying Effective Connectivity of the Cortical Neuroelectric Activity associated with Behavioural Microsleeps”

by Jlenia Toppi, Laura Astolfi, Govinda R. Poudel, Carrie R.H. Innes, Fabio Babiloni, Richard D. Jones

Neuroimage journal, Volume 124, Part A, 1 January 2016, Pages 421-432

<https://doi.org/10.1016/j.neuroimage.2015.08.059>

Time-Varying Effective Connectivity of the Cortical Neuroelectric Activity associated with Behavioural Microsleeps

Jlenia Toppi^{1,2}, Laura Astolfi^{1,2}, Govinda R. Poudel^{3,4}, Carrie R.H. Innes^{5,6}, Fabio Babiloni^{2,7},
Richard D. Jones^{5,6,8,9}

¹ *Department of Computer, Control, and Management Engineering, University of Rome “Sapienza”*

² *Neuroelectrical Imaging and BCI Lab, IRCCS Fondazione Santa Lucia, Rome, Italy*

³ *Monash Biomedical Imaging, Monash University, Melbourne, Australia*

⁴ *School of Psychological Sciences, Monash University, Melbourne, Australia*

⁵ *New Zealand Brain Research Institute, Christchurch, New Zealand*

⁶ *Electrical and Computer Engineering, University of Canterbury, Christchurch, New Zealand*

⁷ *Department of Molecular Medicine, University of Rome “Sapienza”*

⁸ *Medicine, University of Otago, Christchurch, New Zealand*

⁹ *Psychology, University of Canterbury, Christchurch, New Zealand*

Correspondence to: Department of Computer, Control and Management Engineering

University of Rome “Sapienza”

Via Ariosto 25, 00185 Rome, Italy

Neuroelectrical Imaging and BCI Lab

IRCCS Fondazione Santa Lucia

Via Ardeatina 306, 00179 Rome, Italy

E-mail: jlenia.toppi@uniroma1.it

Phone: +39 0651501165

Submitted to: *NeuroImage*

Date: May 2015

Abstract

An episode of complete failure to respond during an attentive task accompanied by behavioural signs of sleep is called a behavioural microsleep. We proposed a combination of high-resolution EEG and an advanced method for time-varying effective connectivity estimation for reconstructing the temporal evolution of the causal relations between cortical regions when microsleeps occur during a continuous visuomotor task. We found connectivity patterns involving left-right frontal, left-right parietal, and left-frontal/right-parietal connections [commencing in the interval \[-500;-250\] ms](#) prior to the onset of microsleeps and disappearing at the end of the microsleeps. Our results from global graph indices derived from effective connectivity analysis have revealed EEG-based biomarkers of all stages of microsleeps (preceding, onset, pre-recovery, recovery). In particular, this raises the possibility of being able to *predict* microsleeps in real-world tasks and initiate a ‘wake-up’ intervention to avert the microsleeps and, hence, prevent injurious and even multi-fatality accidents.

Keywords

Behavioral Microsleeps, Effective Connectivity, Graph Theory, Time-varying connectivity, EEG

1. Introduction

During extended attention-demanding tasks, subjects frequently fail to respond to certain stimuli. Three different types of failures can occur: response error (incorrect response), slowed response (increased reaction time), and absence of any response. An episode of complete failure to respond — lapse of responsiveness (‘lapse’) — accompanied by behavioural signs of drowsiness and slow-eye-closure is known as a behavioural microsleep (‘microsleep’) (Peiris et al., 2006). The occurrence of microsleeps to people working in sectors requiring high vigilance, such as car and truck drivers, locomotive drivers, airline pilots, air traffic controllers, health professionals, and process control workers, can have serious/fatal consequences (Léger et al., 2014; Krahl et al., 2010; Akerstedt, 2000; Summala et al., 1999). For this reason, technology able to detect microsleeps soon after their onset - or, better still, prior to their occurrence - and initiate wake-up warnings, has become an important objective towards helping minimize the occurrence of such accidents.

Early detection and prediction of microsleeps suggests a strong need for the investigation of their neurophysiological correlates.

We have conducted several studies, based on behavioural, functional magnetic resonance imaging (fMRI), and/or electroencephalographic (EEG) data, to determine the neuronal processes underlying microsleeps (Poudel et al., 2014; Innes et al., 2013; Peiris et al., 2011; Jones et al., 2010; Davidson et al., 2007; Peiris et al., 2006). Multiple behavioural cues, including visuomotor responsiveness, eye-closure, head-nodding, and facial video, have been used to identify microsleeps. fMRI studies have revealed a consistent decrease in bilateral thalamic activity associated with loss of arousal (Portas et al., 1998), transition to sleep (Kaufmann et al., 2006), slowed reactions after sleep deprivation (Chee et al., 2008), and microsleeps (Poudel et al., 2014). Decreased activity in the posterior cingulate gyrus and medial frontal cortex, and increased activity in occipito-parietal and frontal areas, are associated with loss of vigilance (Olbrich et al., 2009) and microsleeps (Poudel et al., 2014, 2013, 2009, 2008).

EEG studies have shown increased spectral power in the delta, theta, and alpha bands, and decreased spectral activity in the beta, gamma, and higher bands during drowsiness (Jap et al., 2009; Lin et al., 2005a; Cajochen et al., 1999; Jung et al., 1997). However, there are few correlations between lapses and changes in power spectra (Peiris et al., 2006).

Among the techniques available for the neurophysiological characterization of microsleeps, fMRI has provided the best results in terms of 3-D spatial resolution and localization (Poudel et al., 2009,

2008) while EEG is more desirable in terms of its high temporal resolution (Peiris et al., 2006, 2011; Davidson et al., 2007; Poudel et al., 2010). EEG seems to have the most potential for early detection and prediction of microsleeps in a real-world environment, due to a combination of its high temporal resolution and feasibility, portability, and wearability.

fMRI/EEG studies conducted until now have provided insights in the localization of the cerebral activities associated to the microsleeps, characterizing the spectral content of such activations. However, a description of the temporal evolution of the cerebral phenomena underlying microsleeps, a separate characterization of the mechanisms at the basis of onset and recovery from microsleeps and, most important, a representation of the cerebral circuits (groups of areas communicating each other) involved in such phenomenon are still missing. For this reason, we proposed a combination of high-resolution EEG techniques (Babiloni et al., 2001) and advanced methods for time-varying effective connectivity estimation (Milde et al., 2010) with the aim:

- to improve knowledge on the cerebral mechanisms underlying microsleeps, disentangling different neurophysiological aspects correlated with their the onset and ending;
- to provide biological markers of microsleeps to be used in their early-detection/prediction.

Our approach has allowed us to improve the low spatial resolution of EEG by reconstructing the cortical sources of EEG activity and provide a time-frequency description of the cerebral networks established between different cerebral areas during the occurrence of a microsleep. Estimation of effective connectivity allows us to go beyond results derivable from spectral analysis (Poudel et al., 2014) by providing information on the interaction between different brain areas during each stage of microsleeps (preceding, onset, pre-recovery, recovery). This goes beyond the simple hypothesis of involvement of specific areas in the process by making assumptions on the structure of the neural circuit (effective connectivity) and, more importantly, about its timing.

Effective connectivity is defined as the simplest cerebral circuit describing the causal relations observed experimentally between distinct signals recorded from different cerebral sites (Friston, 1994). Among the different estimators defined in the context of effective connectivity, we selected those based on the concept of Granger Causality (Granger, 1969) which, unlike Structural Equation Modeling (McIntosh, 1998) and the Dynamic Causal Model (Friston et al., 2003), does not require any *a priori* knowledge on the connectivity structure and thus can be used when no specification about the connectivity linkages is available (exploratory tools) (Sato et al., 2009). Partial Directed Coherence (PDC) is a Granger-Causality-based spectral estimator providing the directed influences between any given pair of signals in a multivariate data set (Baccalá and Sameshima, 2001). Several studies have demonstrated the higher accuracy of approaches based on the use of multivariate

models built on original time-series (Kus et al., 2004), being the bivariate approach affected by a high number of false positives due to the impossibility of the method in discarding a common effect on a couple of signals of a third one acquired simultaneously (Blinowska et al., 2004). PDC is also of particular interest because it can distinguish between direct and indirect connectivity flows in the estimated connectivity pattern better than the other multivariate Granger-Causality approaches (Astolfi et al., 2007). The original definition of PDC estimator is based on the hypothesis of stationarity of signals included in the estimation process. As microsleeves are inherently non-stationary phenomena, their characterization requires a time-varying adaptation of PDC, based on the Kalman filter (Milde et al., 2010), which has been recently introduced to follow the temporal evolution of time-varying brain networks.

Thus, the state of the art methodologies for increasing spatial resolution of EEG signals and reconstructing the temporal evolution of cerebral networks were used to reach the aims of this study.

2. Material and Methods

2.1. Participants

Twenty right-handed volunteers (10 male/10 female, mean age 29.3 years (21–45 years)) participated in this study. They had no history of neurological, psychiatric, or sleep disorders. They were asked to refrain from consuming any stimulants or depressants, such as alcohol, caffeine, and nicotine, during the 4 hours prior to the session. Participants had to report a usual time to bed between 10–12 pm and a usual time in bed from 7.0–8.5 hours. Their sleep habits were monitored during the 6 days and 5 nights prior to the experimental session by way of a sleep diary and actigraphy (Actiwatch, Mini Mitter Inc., Bend OR, USA). Ethical approval for the study was obtained from the New Zealand Upper South B Regional Ethics Committee.

2.2. Experimental tasks

Subjects, comfortably lying in a fMRI scanner and wearing a 60-electrodes EEG cap, performed a continuous 2-D tracking task, which was extended, monotonous, and non-stimulating task, and, hence, favours the occurrence of microsleeves even when non-sleep-deprived (Peiris et al., 2006; Poudel et al., 2014; Innes et al., 2013; Poudel et al., 2008; Buckley et al., 2014). Experimental sessions were conducted in post-prandial time (1:30 pm or 2:30 pm), with the aim of facilitating the occurrence of microsleeves. Each participant performed a two-block experiment, comprising a 10-min cued eye-closure task (baseline period), used for simulation of microsleeve-like behaviour, and a

50-min continuous random visuomotor tracking task (microsleeps period). In the continuous tracking task, subjects had to manoeuvre a finger-based joystick (Current Designs, Philadelphia, PA, USA) to pursue a 2-D random target moving continuously on a computer screen (Poudel et al., 2013). Baseline period was designed as an event-related task with an interstimulus time of 12 s, used to pseudo-randomly present 3 s cues for eye-closure and stopping during visuomotor tracking (see Fig.1a and 1b). Each cue was presented 24 times during the experiment. The participants were instructed to close and stop tracking for ‘Stop+Close’ cues and just stop tracking for ‘Stop’ cues. Participants were familiarized with the tracking task and instructed to control the joystick position so that the response disc was as close as possible to the centre of the moving target at all times. See elsewhere for further details on the experimental design (Poudel et al., 2014, 2013).

2.3. Behavioural, EEG and fMRI recordings

Participants performed the tracking task inside an MRI scanner (GE Signa 3.0 T). Joystick response, eye-video, EEG, and fMRI data were recorded synchronously. Video of the right eye was captured using a Visible Eye™ system (Avotec Inc., Stuart FL, USA) mounted on the head-coil of the MRI scanner. The video was recorded on a PC at 25 fps (350 x 280 px) using a video-capture card and custom-built video-recording software.

Continuous EEG was acquired using an MRI-compatible Maglink EEG cap, SynAmps2 amplifiers, and Scan 4.4 software (Compumedics Neuroscan, Charlotte, NC, USA). The Maglink cap has 64 EEG electrodes placed according to an extension of the 10-20 international system, a reference electrode between Cz and Pz, and a ground electrode anterior to Fz. Quick-cell inserts were placed in electrode cavities and soaked with electrolyte solution (0.3 ml) to create a conductive column from the scalp to the electrode. Continuous vertical electrooculogram (VEOG) was acquired by placing electrodes above and below the left eye. Data was acquired at 10 kHz, with a low-pass filter at 2 kHz.

The fMRI side of the study is not discussed further in this paper. Full details on the structural MRI and fMRI methodology can be seen elsewhere (Poudel et al., 2014).

2.4. Identification of Microsleeps

We used well-established behavioural rating criteria to identify individual episodes of microsleeps (Peiris et al., 2006; Poudel et al., 2014, 2012). Briefly, a custom-built SyncPlayer™ program was used to replay synchronized eye-video, VEOG, and tracking target (x and y), response (x and y), speed, and tracking error. Any episodes of flat tracking (zero response speed) of 0.5–15 s duration accompanied by behavioural signs of drowsiness and full or partial (>80%) slow-eye-closures were

marked as microsleeps. The response position, speed, and error signals were used to mark the onset and end of flat tracking responses. Eye-video was used as a cue to mark the onset and end of flat tracking responses.

A minimum inter-microsleep interval of 500 ms was required to ensure that a microsleep's onset is not overlapped with the end of the previous microsleep event. Only microsleeps with a duration ≥ 2 s were included in the study, in order to avoid overlapping of neural mechanisms associated with the onset of a microsleep with those associated with end of a microsleep.

2.5. EEG analysis

2.5.1. Signal pre-processing

Clean EEG was obtained from the continuous artefact-laden EEG collected in the scanner by removing echo-planar gradient artefacts using template subtraction (Allen et al., 2000) and cardio-ballistic artefacts by independent component analysis (ICA) (Briselli et al., 2006).

EEG data were then downsampled to 100 Hz and band-pass filtered (1–45 Hz) to limit the frequency content of acquired signals to the bands of interest. ICA was applied to remove horizontal and vertical eye movements (Hoffmann and Falkenstein, 2008). The analysis was performed on two different time intervals, segmented according to the beginning and the end of the microsleep, respectively. Specifically, EEG traces were segmented into two time windows defined as [-500; 750] ms (ON-phase) and [-750; 500] ms (OFF-phase) relative to the onset and the end of microsleep, respectively (Fig. 1a,b). The ranges of these two temporal windows were defined on the basis of a statistical analysis performed on the distributions achieved for microsleep duration and inter-microsleep interval among all the subjects involved in the experiment. The same segmentation was applied to baseline data (Fig. 1a,b). Residual artefacts were rejected according to a semi-automatic procedure based on the identification of a threshold for the maximum allowed amplitude for EEG signals (± 80 μ V). All trials in which 2 or more channels exceeded such a threshold were excluded from the analysis.

2.5.2. Cortical waveforms reconstruction

The activity of cortical sources was reconstructed, starting from EEG signals acquired at scalp level, by means of the weighted minimum-norm solution for the associated linear inverse problem (Babiloni et al., 2001). The transformation from scalp to cortical domain was performed by means of a realistic head model available from the Montreal Neurologic Institute (Holmes et al., 1998). Then, by averaging the contribution of different sources, the waveforms of 12 cortical regions of

interest (ROIs) (Brodmann Area (ba): 19L/R, 7L/R, 5L/R, 8L/R, 9/46L/R, 10L/R) (Fig. 1c) were derived. Such ROIs were selected on the basis of the fMRI results reported by Poudel et al. (2014).

2.5.3. Connectivity Analysis and Statistical Validation

The estimation of cerebral networks underlying microsleeps was performed by means of time-varying Partial Directed Coherence (Baccalá and Sameshima, 2001; Astolfi et al., 2006, 2008), a spectral multivariate estimator based on Wiener-Granger causality theory (Granger, 1969). The order of the Multivariate Autoregressive model (MVAR) used in the estimate was set to 16. The amount of data available for the estimate guaranteed the accuracy of the process. The number of data observations for each subject was, in fact, much higher than the number of parameters to be estimated in a network comprising 12 nodes.

The time-varying approach was used in the present work in order to follow the time evolution of the estimated circuits during the microsleeps onset and ending. In particular, the reconstructed cortical waveforms were subjected to time-varying effective connectivity estimation via the General Linear Kalman Filter algorithm (Milde et al., 2010; Toppi et al., 2012a). This approach provided accurate sample-by-sample connectivity values within the considered time intervals. High accuracy in the connectivity estimates plus high temporal resolution were ensured by the choice of GLKF forgetting factors equal to 0.3, as suggested by Milde et al. (2010). Selection of these values for the two forgetting factors ensured high temporal resolution in describing all transitions in connectivity patterns occurring in considered EEG epochs lasting 1.5 s. Connectivity patterns elicited during microsleeps were statistically contrasted against those achieved in the baseline, to exclude the effects due to the interruption of tracking task and to the eye-closure. The statistical threshold for PDC estimates was obtained as the 95th percentile of baseline PDC distribution, corrected for multiple comparisons by the False Discovery Rate (Benjamini and Yekutieli, 2001). The significant connectivity values were then averaged in four frequency bands, defined according to the individual alpha frequency (Klimesch, 1999). In particular, we considered two frequency bands: theta [IAF-6; IAF-2] Hz, and alpha [IAF-2; IAF+2] Hz, where IAF = 9.4 ± 0.3 Hz. Beta and gamma bands were excluded from the analysis due to a high number of artefacts and low signal to noise ratio, respectively. We then averaged the sample-by-sample estimates in time intervals defined according to the microsleep event. In particular, the periods [-500 ; 750] ms relative to the onset (ON-PHASE) and the periods [-750 ; 500] relative to the end (OFF-PHASE) of microsleeps were divided into five intervals of equal duration (250 ms) (see Fig. 2 and Fig. 3). Average PDC values in 250-ms time intervals took into account inter-subject variability in the dynamics of brain circuits activated during microsleeps. Such inter-subject variability, typical of physiological processes such as underlying

microsleeps, prevented our exploration of the hypothesis that the temporal evolutions of connectivity networks are aligned both within and between healthy subjects.

Secondly, the reduction of the number of points in which statistical comparisons between real and random networks were performed (i.e., 6 points corresponding to 6 time intervals instead of the 150 corresponding to the data samples included in the EEG epochs) ensured more accurate and sensitive results due to not being affected by family-wise error rate. Moreover, under-sampling of the estimated patterns smoothed the trends achieved for graph indices, hence reducing the random oscillations of their values and providing more stable values for statistical analysis.

2.5.4. Statistical group analysis of connectivity patterns

To summarize the results achieved on single participants and to obtain the network characterizing microsleep events, we performed a group analysis consisting of a statistical comparison between microsleeps and baseline networks, computed along the population (paired t -test, significance level 5%). Such comparison was repeated for each frequency band and for the two microsleeps phases (ON and OFF), separately. False Discovery Rate correction was applied in order to reduce the occurrence of false positives. Such group analysis allowed to achieve the group statistical patterns showed in Fig.2 and Fig.3, where we reported only the connections differing in the population from the baseline.

2.5.5. Graph Theory Analysis

To describe and quantify the connectivity patterns obtained by time-varying PDC, we computed a number of indices derived from graph theory applied to the brain networks. The statistical approach here adopted for the validation of connectivity networks allowed to extract adjacency matrices (describing the internal structure of the network being investigated) for the computation of graph indices, avoiding the alterations of the real topological properties of the networks that may arise applying empirical approaches as demonstrated by Toppi et al. (Toppi et al., 2012b).

The adjacency matrix is a mathematical representation of a network, used in graph to extract salient indices characterizing network properties. The generic ij^{th} entry of a directed binary adjacency matrix is equal to 1 if there is an effective link directed from the j^{th} to the i^{th} signal and is equal to 0 if no links exist. The adjacency matrix can be built by comparing each connectivity value A_{ij} with its corresponding threshold value τ_{ij} . In particular:

$$G_{ij} = \begin{cases} 1 & \rightarrow A_{ij} \geq \tau_{ij} \\ 0 & \rightarrow A_{ij} < \tau_{ij} \end{cases}, \quad (1)$$

where G_{ij} and A_{ij} represent the entry (i, j) of the adjacency matrix G and the connectivity matrix A , respectively, and τ_{ij} is the corresponding threshold. Different approaches have been developed for evaluating the threshold values, most of them based on qualitative assumptions aiming at fixing the edge density in the network or the degree of some nodes or at maximizing small-world properties of the investigated networks. In this study we used a statistical approach in which the threshold τ_{ij} corresponds to the 95th percentile (corrected by False Discovery Rate for multiple comparisons) of PDC distribution achieved in the baseline condition. The use of a statistical threshold for the extraction of the adjacency matrix has been demonstrated superior to an empirical approach by avoiding alterations to real topological properties of investigated networks (Toppi et al., 2012b).

In the present study, we considered two sets of indices, the first describing integration and segregation properties of the investigated networks (global indices), the second characterizing the involvement and the role of specific ROIs (local indices).

Global Indices

Characteristic Path Length - defined as:

$$L = \frac{1}{n} \sum_{i \in N} L_i = \frac{1}{n(n-1)} \sum_{\substack{i, j \in N \\ i \neq j}} d_{ij} , \quad (2)$$

where L_i is the average distance between node i and all other nodes and d_{ij} is the distance between node i and node j . N represents the number of nodes in the graph. The Characteristic Path Length is also defined as the average shortest path length in the network. The shortest path length (geodesic distance) between two nodes is the minimum number of connections linking two regions (Sporns et al., 2004).

Global Efficiency —defined as:

$$E_g = \frac{1}{N(N-1)} \sum_{i \neq j} \frac{1}{d_{ij}} , \quad (3)$$

where N represents the number of nodes in the graph and d_{ij} the geodesic distance between i and j .

It is defined as the average of the inverse of the geodesic length and represents the efficiency of the communication between all the nodes in the network (Latora and Marchiori, 2001).

Local Efficiency — defined as:

$$E_i = \frac{1}{N} \sum_{i=1}^N E_g(S_i) , \quad (4)$$

where N represents the number of nodes in the graph and S_i the sub-graph achieved by deleting the i^{th} row and the i^{th} column from the original graph.

It is the average of the global efficiencies computed on each sub-graph belonging to the network and represents the efficiency of communication between all nodes around node i in the network (Latora and Marchiori, 2001).

Clustering Coefficient— defined as:

$$C = \frac{1}{n} \sum_{i \in N} C_i = \frac{1}{n} \sum_{i \in N} \frac{t_i}{(k_i^{\text{out}} + k_i^{\text{in}})(k_i^{\text{out}} + k_i^{\text{in}} - 1) - 2 \sum_{j \in N} G_{ij} G_{ji}} , \quad (5)$$

where t_i represents the number of triangles involving node i , k_i^{in} and k_i^{out} are the number of incoming and outgoing edges of nodes i respectively, and G_{ij} is the entry ij of adjacency matrix G .

It describes the intensity of inter-connections between the neighbours of a node (Watts and Strogatz, 1998). It is defined as the fraction of triangles around a node or the fraction of a node's neighbours that are neighbours of each other (Fagiolo, 2007).

Small-Worldness — A network G is defined as a Small-World network if $L_G \geq L_{\text{rand}}$ and $C_G \gg C_{\text{rand}}$, where L_G and C_G represent the characteristic path length and the clustering coefficient of a generic graph and L_{rand} and C_{rand} represent the corresponding quantities for a random graph. On the basis of this definition, a measure of Small-Worldness of a network can be defined as

$$SW = \frac{C_G / C_{\text{rand}}}{L_G / L_{\text{rand}}} , \quad (6)$$

A network has the property of *small worldness* if $SW > 1$.

It is also defined as a measure of the level of organization in a network (Watts and Strogatz, 1998). In this paper we used the formulation of (Humphries and Gurney, 2008).

To be validated against the null case, the values achieved for global indices characterizing the connectivity networks (local efficiency, clustering coefficient, Small-Worldness) were statistically compared (independent samples t-test, $p < 0.05$) with those computed on 50 random graphs generated by imposing the same number of connections of the corresponding real networks,

randomly shuffled among all possible positions in the network. Such an approach provided assurance that the differences in graph indexes found between different phases of the microsleeps were not due to differences in the density of the corresponding estimated networks.

Local Indices

Density — defined as

$$k = \left(\frac{1}{N(N-1)} \sum_{i=1}^N \sum_{j=1}^N G_{ij} \right) \cdot 100 , \quad (7)$$

where N is the number of nodes in the network and G_{ij} represents the entry (i, j) of the adjacency matrix G .

It is defined as the percentage of existing connections in a network over the total. The density index can also be computed on particular sub-networks extracted from the complete network. In the present work, we computed the density index in cortical regions located in the anterior part of the brain (anterior density) or right hemisphere (right density). In particular, for the computation of anterior density and right density indices we considered anterior areas to comprise ba10L, ba8L, ba9/46L, ba10R, ba8R, and ba9/46R, and right hemisphere areas to comprise ba10R, ba8R, ba5R, ba7R, ba19R, and ba9/46R.

Degree— defined as

$$w_f = \sum_{j \in N, j \neq f} G_{fj} + \sum_{i \in N, i \neq f} G_{if} , \quad (8)$$

where g_{ij} represents the entry ij of the adjacency matrix G .

The degree of each node is the number of links connected directly to that node. In directed networks, the in-degree of a specific brain region is the number of inward links and the out-degree is the number of outward links (Sporns et al., 2004).

The values achieved for global indices (local efficiency, clustering coefficient, Small-Worldness) were statistically compared (independent samples t-test, $p < 0.05$) with those computed on 50 random graphs generated by imposing the same number of connections of the corresponding real networks (van Wijk et al., 2010).

3. Results

3.1. Behavioural Microsleeps

Twenty subjects were involved in the study, among which 14 had frequent microsleeps (≥ 36 during the 50 min of recording) and, of these, 10 had reasonably good 64-channel EEG (the other 4 had too many serious artefacts). Thus, we report here the results obtained from these 10 subjects (6 males / 4 females, mean age 30.4 years). They had an average of 89.0 microsleeps (36–188) with a mean average duration of 3.6 s (1.3–6.3 s).

3.2. Connectivity Analysis

Time-varying connectivity patterns elicited during the ON-phase in the group of subjects are shown in Fig. 2a and 2c, for theta and alpha bands, respectively (see Methods for details about the estimation of time-varying connectivity and the statistical group analysis). As for the theta band, the cortical patterns in Fig. 2a reveal a connectivity network, statistically different from the baseline condition, commencing 500 ms prior to the onset of the microsleep. From 250 ms before the microsleep onset we see a pattern which reinforces during the microsleep. In particular, we found two connectivity patterns, one composed by fronto-parietal connections, mainly involving right-parietal/left-frontal areas starting [in the interval \[-500;-250\]ms](#) before microsleep onset and one involving right-parietal/right-frontal areas 250 ms before microsleep onset. A close communication within frontal areas (left and right hemispheres) commences [in the interval \[-500;-250\] ms](#) before microsleep onset and persists during the microsleep, whereas a strong inter-connection between parieto-occipital areas occurs immediately following the microsleep onset.

In order to highlight the role of each cortical region in the elicited networks, we have also represented the in-degree and out-degree indices of each ROI on the same cortex model (see Methods for details about the degree computation). The degree analysis results for the ON-phase are shown in Fig. 2b and 2d, for theta and alpha bands. In particular, results in theta (Fig. 2b) points out a role of right parieto-occipital areas, mainly ba7R, as main target of information flows (high in-degree) and a role of left frontal areas as main driver of the network (high out-degree). This is kept for all the microsleep duration. Moreover, ba10R shows a role as main target of information flows in the interval [-250 ; 500] ms according to the microsleep onset. Taken all together, these results highlight the existence of a fronto-parietal network directed from bilateral frontal regions (mainly left) to right parieto-occipital cortical areas. Such network is established before and during the microsleep event. Results in alpha band confirm the same patterns and the corresponding role of considered ROIs (see Fig.2c-d).

The results of the group analysis performed, as described in Methods section, on connectivity patterns elicited during the OFF-phase in theta and alpha bands are shown in Fig.3a-3c. The cortical networks resulting in the period [-750 ; 0] ms according to the end microsleeper confirm the pattern obtained after the microsleeper onset (right-parietal/left-frontal areas and right-parietal/right-frontal areas). Moreover, in the interval [-250 ; 0] ms before the end of microsleeper, the connection between ba9/46_L and ba10_R disappears.

Fronto-parietal connections persist up to 250 ms beyond the end of the microsleeper and then slowly disappear. The degree analysis results (Fig. 3b–3d) point out an involvement of left frontal areas (ba9/46L, ba10L) similar to the one obtained during the ON-phase. Such role is gradually reduced toward the end of the microsleeper until its disappearance. A similar behaviour is found for ba7_R.

3.3. Graph Theory Analysis

Local Indices

To further investigate the properties of the networks obtained by the connectivity analysis, specific graph theory indices are computed (see Methods for mathematical details about the graph indices adopted). Fig. 4a,c shows an increase of the anterior density and right density indices along the five time intervals analysed during the ON-phase. The same indices decreased in the window around the end of a microsleeper in the OFF-phase (Fig. 4b,d).

Global Indices

Fig. 5 shows the results of a statistical comparison between the local efficiency index (see Online Methods) computed during microsleeper onset and conclusion, and correspondent random networks, in the theta band. In particular, significant differences between real and random networks resulted in the 0–250-ms interval following the microsleeper onset (Fig. 5a) with a higher local efficiency of the microsleeper network with respect to random networks. A substantial decrease in the local efficiency index can be seen toward the end of the microsleeper (Fig. 5b). This index is significantly higher than that of random networks until ~250 ms prior to the end of the microsleeper.

Results related to the clustering coefficient index are reported in Fig. 6, and show significantly higher values for real networks with respect to the random ones in all of the intervals, with an increase along the microsleeper onset. In contrast, a decreasing trend can be seen during the OFF-

phase. Significant differences between microsleep and random networks are observed during the microsleep and disappear immediately after.

Finally, results related to the Small-Worldness index are reported in Fig.7, and show a trend similar to the clustering coefficient.

Similar results for all the indices here reported were obtained for the alpha band.

4. Discussion

This paper is the first to report on changes in time and frequency characteristics of the information flow between multiple cortical areas during spontaneous behavioural microsleeps. This could be achieved by the use of advanced methods for the estimation of time-varying effective connectivity in conjunction with the knowledge about the physiological correlates of microsleeps from previous studies.

Spatial characterization of microsleeps

The current EEG data were collected simultaneously with fMRI (Poudel et al., 2014). Results of fMRI analysis performed on this experiment and reported elsewhere (Poudel et al., 2014) revealed decreased activation associated with microsleeps in several brain regions bilaterally, including the midbrain, thalamus, posterior cingulate cortex, and occipital cortex, and small clusters in the right prefrontal cortex and cerebellum. At the same time, fMRI revealed increased activation in several cortical areas, particularly in parietal regions encompassing the bilateral postcentral, superior parietal, and supramarginal cortices. Although fMRI has provided immensely valuable insight into the 3-D spatial attributes of microsleeps (Poudel et al., 2014), its relatively long sampling interval (2.5 s) seriously limits its ability to reveal spatiotemporal aspects of neural activity related to microsleeps. In contrast, the high temporal resolution of EEG, together with the powerful multivariate analysis of connectivity, goes a long way to fill this gap by identifying time-resolved information flow between different key areas in the cortex.

Spectral characterization of microsleeps

A previous study (Peiris et al., 2006) showed that microsleeps during an extended continuous visuomotor task, similar to the one we used in the current study, are associated with increased power and positive correlations in the delta, theta, and alpha bands and decreased power in the beta, gamma, and higher bands, even if the correlations between EEG band power and definite microsleeps are low. Other studies have shown a correlation between theta activity and drops in performance on a pursuit tracking task (Poudel et al., 2010) and a simulated driving task (Lin et al.,

2005a). The theta and alpha bands, moreover, are involved in cerebral processes related to alertness, attention and their loss due to pathological or fatigue phenomena (Chua et al., 2014; Song et al., 2014; Wascher et al., 2014). The connectivity analysis performed in the present study was therefore focused on theta and alpha bands.

Connectivity Analysis

In contrast to the studies focusing on changes in the EEG spectral power during lapses, the focus of the present study was on determining time-frequency changes in causal connections between cortical areas. By comparison with baseline connectivity during alert performance, we revealed characteristic connectivity patterns in the theta and alpha bands arising immediately following and, importantly, prior to the onset of a microsleep.

We focused on both the microsleep onset and its transition to awakening. As for the microsleep onset, we can observe a characteristic connectivity pattern establishing prior to the behavioural signs of microsleeps occurrence and persisting for the entire duration of the event. As for the transition to awakening, characteristic changes in connectivity patterns were observed prior to, and following, the behavioural end of microsleeps. These changes clearly reflect the neural processes and mechanisms (in terms of information flow) underlying recovery from microsleeps.

Our connectivity results show how the areas identified by fMRI studies as involved in microsleep processes (Poudel et al., 2014) communicate with each other before, during, and after microsleeps. To our knowledge, such description of the circuit underlying the process of microsleeps is unprecedented in literature, as well as the definition of markers, based on brain networks properties, able to track the process of microsleep in time with the resolution of milliseconds.

Three sub-networks were mainly associated with microsleeps:

- 1) Left-frontal/right-frontal - This network is associated with the period of 500 ms preceding the microsleep, persists for the duration of the event and reduces toward the end of microsleep. The involvement of frontal areas in microsleeps indicates a residual activity of these areas which usually deactivate during non-REM sleep, as demonstrated by PET (Achermann et al., 2001; Maquet et al., 1997). The increase of anterior density index along the temporal evolution of microsleep events supports this finding.
- 2) Right-parietal/left-frontal - This network, too, appears [in the interval \[-500;-250\]ms](#) before the event onset, persists for the duration of the microsleep and characterizes both the beginning and the end of the event. The presence of an increase of fronto-parietal network is an important feature which allows the distinction between microsleeps and all the other

levels of sleep. In fact, several neuroimaging studies have demonstrated the reduction of fronto-parietal connections, until their complete disruption, in accordance with the level of sleep depth (Spoormaker et al., 2012; Sämann et al., 2011; Horovitz et al., 2008). Network modularity (a measure of functional segregation) has been found to increase during deeper sleep stages highlighting the interruption of communication between frontal and parietal areas (Tagliazucchi et al., 2013).

- 3) Right-parietal/right-frontal - This sub-network appears in the interval [-250;0] ms before microsleep onset and persists for the duration of the event. The strong involvement of the right hemisphere before and during the microsleep event, in the theta band, could be attributed to the loss of attention during microsleep, being such hemisphere associated to this important cognitive function (Asplund et al., 2010; Corbetta and Shulman, 2002).

Subsequent analysis of the connectivity network features by graph analysis allowed the synthesis of all the information reported in the estimated networks and characterization of their main properties. In particular, we found an increase in the Small-World index associated with the temporal evolution of the microsleep event. This feature of microsleep networks is in agreement with results reported by Ferri and colleagues who used graph theory to examine functional connectivity from EEG recordings of spontaneous activity in sleep. In particular, they found a Small-World-like network in sleep in theta and alpha bands (Ferri et al., 2008, 2007). The increase of local efficiency during microsleep onset and its decrease at the end of the event is consistent with networks associated with sleep, maintaining an optimal and efficient functional structure (Koenis et al., 2013). The increase of the clustering coefficient along microsleeps can be interpreted as a modification of the hierarchical organization of large-scale networks into smaller independent modules. Such result is consistent with the dynamics of effective connectivity and the emergence of functional clusters while recording spontaneous EEG activity during sleep (Dimitriadis et al., 2009).

The time-varying approach led to identification and temporal characterization of the networks associated with the occurrence of and recovery from microsleeps. Probably of greatest real-world importance is the presence of changes in connectivity patterns seen up to 500 ms *prior* to microsleeps. That there are characteristic changes in brain activity preceding microsleeps, when one is struggling to counter the overpowering homeostatic urge of the brain to take a rest/nap from the current active task, is not surprising. In fact, Davidson et al. (2007), using a long short-term memory (LSTM) recurrent neural network, showed that information in the EEG spectra up to ~4 s prior to a microsleep can be used to improve microsleep detection. This raises the possibility of being able to use multi-channel EEG to predict the onset of microsleeps and, hence, initiate, say,

auditory or vibratory stimuli to arouse the user and prevent the occurrence of the microsleep and, in turn, potentially prevent a injurious/fatal/multi-fatality lapse of responsiveness in a vehicle-driver, pilot, air-traffic controller, anaesthetist, machine operator, or military personnel. Although we were able to reveal connectivity changes up to 500 ms preceding the onset of microsleeps, this does not exclude the possibility of changes having occurred even earlier, as we had somewhat arbitrarily chosen a minimum inter-microsleep-interval of 500 ms in our study. Further studies are needed to systematically investigate the dimension of the temporal window in which such microsleeps could be predicted. While preliminary, and needing replication in a larger sample, the EEG-based findings from this paper, together with findings from fMRI-based studies (Poudel et al., 2014), contribute substantially to our understanding of the neural mechanisms underlying the often fatal phenomena of microsleeps.

In conclusion, the application of advanced methodologies for cortical sources reconstruction, time-varying connectivity estimation, and graph theory analysis has led to improve the understanding of neurophysiological basis of microsleep events. In fact, this combination of methodologies allowed the spatial limitations of EEG technique to be minimized while maximizing the benefits of its high temporal resolution, so as to provide a spatio-temporal characterization of microsleep events. In summary, microsleep networks are characterized by an involvement of frontal and fronto-parietal sub-networks. In addition, the networks are asymmetric in favour of the right hemisphere, show Small-World properties, and tend to create clusters. The high temporal resolution of EEG and thus of the time-varying approach for effective connectivity estimation allowed us to follow the temporal evolution of microsleep events and to find a set of neurophysiological features that could potentially be used as predictors of behavioural microsleeps.

5. Acknowledgements

The data analyzed in this paper was collected for a project which was funded by a New Zealand Lottery Health Research grant, a University of Otago postgraduate scholarship, and a Christchurch Neurotechnology Research Programme scholarship. LA and JT are supported by a fund by the Italian Ministry of Education, Project FIRB 2013 (Fondo per gli Investimenti della Ricerca di Base-Futuro in Ricerca) - RBF136E24 and by the University of Rome Sapienza “Progetti di Ateneo per la Ricerca Scientifica anno 2014”.

6. References

- Achermann, P., Finelli, L.A., Borbély, A.A., 2001. Unihemispheric enhancement of delta power in human frontal sleep EEG by prolonged wakefulness. *Brain Res.* 913, 220–223. doi:10.1016/S0006-8993(01)02796-2
- Akerstedt, T., 2000. Consensus statement: fatigue and accidents in transport operations. *J. Sleep Res.* 9, 395.
- Allen, P.J., Josephs, O., Turner, R., 2000. A method for removing imaging artifact from continuous EEG recorded during functional MRI. *NeuroImage* 12, 230–239. doi:10.1006/nimg.2000.0599
- Asplund, C.L., Todd, J.J., Snyder, A.P., Marois, R., 2010. A central role for the lateral prefrontal cortex in goal-directed and stimulus-driven attention. *Nat. Neurosci.* 13, 507–512. doi:10.1038/nn.2509
- Astolfi, L., Cincotti, F., Mattia, D., De Vico Fallani, F., Tocci, A., Colosimo, A., Salinari, S., Marciani, M.G., Hesse, W., Witte, H., Ursino, M., Zavaglia, M., Babiloni, F., 2008. Tracking the time-varying cortical connectivity patterns by adaptive multivariate estimators. *IEEE Trans. Biomed. Eng.* 55, 902–913. doi:10.1109/TBME.2007.905419
- Astolfi, L., Cincotti, F., Mattia, D., Marciani, M.G., Baccalà, L.A., de Vico Fallani, F., Salinari, S., Ursino, M., Zavaglia, M., Babiloni, F., 2006. Assessing cortical functional connectivity by partial directed coherence: simulations and application to real data. *IEEE Trans. Biomed. Eng.* 53, 1802–1812. doi:10.1109/TBME.2006.873692
- Astolfi, L., Cincotti, F., Mattia, D., Marciani, M.G., Baccala, L.A., de Vico Fallani, F., Salinari, S., Ursino, M., Zavaglia, M., Ding, L., Edgar, J.C., Miller, G.A., He, B., Babiloni, F., 2007. Comparison of different cortical connectivity estimators for high-resolution EEG recordings. *Hum. Brain Mapp.* 28, 143–157. doi:10.1002/hbm.20263
- Babiloni, F., Carducci, F., Cincotti, F., Del Gratta, C., Pizzella, V., Romani, G.L., Rossini, P.M., Tecchio, F., Babiloni, C., 2001. Linear inverse source estimate of combined EEG and MEG data related to voluntary movements. *Hum. Brain Mapp.* 14, 197–209.
- Baccalà, L.A., Sameshima, K., 2001. Partial directed coherence: a new concept in neural structure determination. *Biol. Cybern.* 84, 463–474. doi:10.1007/PL00007990
- Benjamini, Y., Yekutieli, D., 2001. The Control of the False Discovery Rate in Multiple Testing under Dependency. *Ann. Stat.* 29, 1165–1188.

- Blinowska, K.J., Kuś, R., Kamiński, M., 2004. Granger causality and information flow in multivariate processes. *Phys. Rev. E Stat. Nonlin. Soft Matter Phys.* 70, 050902.
- Briselli, E., Garreffa, G., Bianchi, L., Bianciardi, M., Macaluso, E., Abbafati, M., Grazia Marciani, M., Maraviglia, B., 2006. An independent component analysis-based approach on ballistocardiogram artifact removing. *Magn. Reson. Imaging* 24, 393–400. doi:10.1016/j.mri.2006.01.008
- Buckley, R., Helton, W., Innes, C.R., Dalrymple-Alford, J., Jones, R., 2014. Sustained attention lapses and behavioural microsleeps during tracking, psychomotor vigilance, and dual tasks. *Sleep* 37(Abstract Supplement), A51–52.
- Cajochen, C., Khalsa, S.B., Wyatt, J.K., Czeisler, C.A., Dijk, D.J., 1999. EEG and ocular correlates of circadian melatonin phase and human performance decrements during sleep loss. *Am. J. Physiol.* 277, R640–649.....
- Chee, M.W.L., Tan, J.C., Zheng, H., Parimal, S., Weissman, D.H., Zagorodnov, V., Dinges, D.F., 2008. Lapsing during sleep deprivation is associated with distributed changes in brain activation. *J. Neurosci. Off. J. Soc. Neurosci.* 28, 5519–5528. doi:10.1523/JNEUROSCI.0733-08.2008
- Chua, E.C.-P., Yeo, S.-C., Lee, I.T.-G., Tan, L.-C., Lau, P., Cai, S., Zhang, X., Puvanendran, K., Gooley, J.J., 2014. Sustained attention performance during sleep deprivation associates with instability in behavior and physiologic measures at baseline. *Sleep* 37, 27–39. doi:10.5665/sleep.3302
- Corbetta, M., Shulman, G.L., 2002. Control of goal-directed and stimulus-driven attention in the brain. *Nat Rev Neurosci* 3, 201–215. doi:10.1038/nrn755
- Davidson, P.R., Jones, R.D., Peiris, M.T.R., 2007. EEG-based lapse detection with high temporal resolution. *IEEE Trans. Biomed. Eng.* 54, 832–839. doi:10.1109/TBME.2007.893452
- Dimitriadis, S.I., Laskaris, N.A., Del Rio-Portilla, Y., Koudounis, G.C., 2009. Characterizing dynamic functional connectivity across sleep stages from EEG. *Brain Topogr.* 22, 119–133. doi:10.1007/s10548-008-0071-4
- Fagiolo, G., 2007. Clustering in complex directed networks. *Phys Rev E Stat Nonlin Soft Matter Phys* 76, 026107.
- Ferri, R., Rundo, F., Bruni, O., Terzano, M.G., Stam, C.J., 2008. The functional connectivity of different EEG bands moves towards small-world network organization during sleep. *Clin Neurophysiol* 119, 2026–2036. doi:10.1016/j.clinph.2008.04.294

- Ferri, R., Rundo, F., Bruni, O., Terzano, M.G., Stam, C.J., 2007. Small-world network organization of functional connectivity of EEG slow-wave activity during sleep. *Clin. Neurophysiol. Off. J. Int. Fed. Clin. Neurophysiol.* 118, 449–456. doi:10.1016/j.clinph.2006.10.021
- Friston, K.J., Harrison, L., Penny, W., 2003. Dynamic causal modelling. *NeuroImage* 19, 1273–1302.
- Granger, C.W.J., 1969. Investigating Causal Relations by Econometric Models and Cross-spectral Methods. *Econometrica* 37, 424–438.
- Hoffmann, S., Falkenstein, M., 2008. The correction of eye blink artefacts in the EEG: a comparison of two prominent methods. *PloS One* 3, e3004. doi:10.1371/journal.pone.0003004
- Holmes, C.J., Hoge, R., Collins, L., Woods, R., Toga, A.W., Evans, A.C., 1998. Enhancement of MR images using registration for signal averaging. *J. Comput. Assist. Tomogr.* 22, 324–333.
- Horowitz, S.G., Fukunaga, M., de Zwart, J.A., van Gelderen, P., Fulton, S.C., Balkin, T.J., Duyn, J.H., 2008. Low frequency BOLD fluctuations during resting wakefulness and light sleep: a simultaneous EEG-fMRI study. *Hum. Brain Mapp.* 29, 671–682. doi:10.1002/hbm.20428
- Humphries, M.D., Gurney, K., 2008. Network “small-world-ness”: a quantitative method for determining canonical network equivalence. *PloS One* 3, e0002051. doi:10.1371/journal.pone.0002051
- Innes, C.R.H., Poudel, G.R., Jones, R.D., 2013. Efficient and regular patterns of nighttime sleep are related to increased vulnerability to microsleeps following a single night of sleep restriction. *Chronobiol. Int.* 30, 1187–1196. doi:10.3109/07420528.2013.810222
- Jap, B.T., Lal, S., Fischer, P., Bekiaris, E., 2009. Using EEG spectral components to assess algorithms for detecting fatigue. *Expert Syst. Appl.* 36, 2352–2359. doi:10.1016/j.eswa.2007.12.043
- Jones, R.D., Poudel, G.R., Innes, C.R.H., Davidson, P.R., Peiris, M.T.R., Malla, A.M., Signal, T., Carroll, G.J., Watts, R., Bones, P.J., 2010. Lapses of responsiveness: Characteristics, detection, and underlying mechanisms. *Conf. Proc. Annu. Int. Conf. IEEE Eng. Med. Biol. Soc. IEEE Eng. Med. Biol. Soc. Conf.* 2010, 1788–1791. doi:10.1109/IEMBS.2010.5626385
- Jung, T.P., Makeig, S., Stensmo, M., Sejnowski, T.J., 1997. Estimating alertness from the EEG power spectrum. *IEEE Trans. Biomed. Eng.* 44, 60–69. doi:10.1109/10.553713
- Kaufmann, C., Wehrle, R., Wetter, T.C., Holsboer, F., Auer, D.P., Pollmächer, T., Czisch, M., 2006. Brain activation and hypothalamic functional connectivity during human non-rapid

- eye movement sleep: an EEG/fMRI study. *Brain J. Neurol.* 129, 655–667. doi:10.1093/brain/awh686
- Klimesch, W., 1999. EEG alpha and theta oscillations reflect cognitive and memory performance: a review and analysis. *Brain Res Brain Res Rev* 29, 169–195.
- Koenis, M.M.G., Romeijn, N., Piantoni, G., Verweij, I., Van der Werf, Y.D., Van Someren, E.J.W., Stam, C.J., 2013. Does sleep restore the topology of functional brain networks? *Hum. Brain Mapp.* 34, 487–500. doi:10.1002/hbm.21455
- Krahl, P.L., Jankosky, C.J., Thomas, R.J., Hooper, T.I., 2010. Systematic review of military motor vehicle crash-related injuries. *Am. J. Prev. Med.* 38, S189–196. doi:10.1016/j.amepre.2009.10.024
- Kus, R., Kaminski, M., Blinowska, K.J., 2004. Determination of EEG activity propagation: pairwise versus multichannel estimate. *IEEE Trans. Biomed. Eng.* 51, 1501–1510. doi:10.1109/TBME.2004.827929
- Latora, V., Marchiori, M., 2001. Efficient behavior of small-world networks. *Phys. Rev. Lett.* 87, 198701.
- Léger, D., Bayon, V., Ohayon, M.M., Philip, P., Ement, P., Metlaine, A., Chennaoui, M., Faraut, B., 2014. Insomnia and accidents: cross-sectional study (EQUINOX) on sleep-related home, work and car accidents in 5293 subjects with insomnia from 10 countries. *J. Sleep Res.* 23, 143–152. doi:10.1111/jsr.12104
- Lin, C.T., Wu, R.C., Jung, T.P., Liang, S.F., Huang, T.Y., 2005a. Estimating driving performance based on EEG spectrum analysis. *EURASIP J. Appl. Signal Process.* 19, 3165–3174.
- Maquet, P., Degueldre, C., Delfiore, G., Aerts, J., Péters, J.M., Luxen, A., Franck, G., 1997. Functional neuroanatomy of human slow wave sleep. *J. Neurosci. Off. J. Soc. Neurosci.* 17, 2807–2812.
- McIntosh, A.R., 1998. Understanding neural interactions in learning and memory using functional neuroimaging. *Ann. N. Y. Acad. Sci.* 855, 556–571.
- Milde, T., Leistritz, L., Astolfi, L., Miltner, W.H.R., Weiss, T., Babiloni, F., Witte, H., 2010. A new Kalman filter approach for the estimation of high-dimensional time-variant multivariate AR models and its application in analysis of laser-evoked brain potentials. *NeuroImage* 50, 960–969. doi:10.1016/j.neuroimage.2009.12.110
- Olbrich, S., Mulert, C., Karch, S., Trenner, M., Leicht, G., Pogarell, O., Hegerl, U., 2009. EEG-vigilance and BOLD effect during simultaneous EEG/fMRI measurement. *NeuroImage* 45, 319–332. doi:10.1016/j.neuroimage.2008.11.014

- Peiris, M.T.R., Davidson, P.R., Bones, P.J., Jones, R.D., 2011. Detection of lapses in responsiveness from the EEG. *J. Neural Eng.* 8, 016003. doi:10.1088/1741-2560/8/1/016003
- Peiris, M.T.R., Jones, R.D., Davidson, P.R., Carroll, G.J., Bones, P.J., 2006. Frequent lapses of responsiveness during an extended visuomotor tracking task in non-sleep-deprived subjects. *J. Sleep Res.* 15, 291–300. doi:10.1111/j.1365-2869.2006.00545.x
- Portas, C.M., Rees, G., Howseman, A.M., Josephs, O., Turner, R., Frith, C.D., 1998. A specific role for the thalamus in mediating the interaction of attention and arousal in humans. *J. Neurosci. Off. J. Soc. Neurosci.* 18, 8979–8989.
- Poudel, G.R., Innes, C.R.H., Bones, P.J., Jones, R.D., 2010. The relationship between behavioural microsleeps, visuomotor performance and EEG theta. *Conf. Proc. Annu. Int. Conf. IEEE Eng. Med. Biol. Soc.* 2010, 4452–4455. doi:10.1109/IEMBS.2010.5625956
- Poudel, G.R., Innes, C.R.H., Bones, P.J., Watts, R., Jones, R.D., 2014. Losing the struggle to stay awake: divergent thalamic and cortical activity during microsleeps. *Hum. Brain Mapp.* 35, 257–269. doi:10.1002/hbm.22178
- Poudel, G.R., Innes, C.R.H., Jones, R.D., 2013. Distinct neural correlates of time-on-task and transient errors during a visuomotor tracking task after sleep restriction. *NeuroImage* 77, 105–113. doi:10.1016/j.neuroimage.2013.03.054
- Poudel, G.R., Innes, C.R.H., Jones, R.D., 2012. Cerebral perfusion differences between drowsy and nondrowsy individuals after acute sleep restriction. *Sleep* 35, 1085–1096. doi:10.5665/sleep.1994
- Poudel, G.R., Jones, R.D., Innes, C.R.H., Davidson, P.R., Watts, R., Signal, T., Bones, P.J., 2008. Functional-MRI correlates of cued slow-eye-closure and task non-responsiveness during visuomotor tracking. *Conf. Proc. Annu. Int. Conf. IEEE Eng. Med. Biol. Soc. IEEE Eng. Med. Biol. Soc. Conf.* 2008, 4122–4125. doi:10.1109/IEMBS.2008.4650116
- Poudel, G.R., Jones, R.D., Innes, C.R.H., Watts, R., Signal, T.L., Bones, P.J., 2009. fMRI correlates of behavioural microsleeps during a continuous visuomotor task. *Conf. Proc. IEEE Eng. Med. Biol. Soc.* 2009, 2919–2922. doi:10.1109/IEMBS.2009.5334486
- Sämman, P.G., Wehrle, R., Hoehn, D., Spoormaker, V.I., Peters, H., Tully, C., Holsboer, F., Czisch, M., 2011. Development of the brain's default mode network from wakefulness to slow wave sleep. *Cereb. Cortex N. Y. N* 1991 21, 2082–2093. doi:10.1093/cercor/bhq295
- Sato, J.R., Takahashi, D.Y., Arcuri, S.M., Sameshima, K., Morettin, P.A., Baccalá, L.A., 2009. Frequency domain connectivity identification: An application of partial directed coherence in fMRI. *Hum. Brain Mapp.* 30, 452–461. doi:10.1002/hbm.20513

- Song, K., Meng, M., Chen, L., Zhou, K., Luo, H., 2014. Behavioral oscillations in attention: rhythmic α pulses mediated through θ band. *J. Neurosci. Off. J. Soc. Neurosci.* 34, 4837–4844. doi:10.1523/JNEUROSCI.4856-13.2014
- Spoormaker, V.I., Gleiser, P., Czisch, M., 2012. Frontoparietal connectivity and hierarchical structure of the brain's functional network during sleep. *Sleep Chronobiol.* 3, 80. doi:10.3389/fneur.2012.00080
- Sporns, O., Chialvo, D.R., Kaiser, M., Hilgetag, C.C., 2004. Organization, development and function of complex brain networks. *Trends Cogn. Sci.* 8, 418–425. doi:10.1016/j.tics.2004.07.008
- Summala, H., Häkkinen, H., Mikkola, T., Sinkkonen, J., 1999. Task effects on fatigue symptoms in overnight driving. *Ergonomics* 42, 798–806. doi:10.1080/001401399185298
- Tagliazucchi, E., von Wegner, F., Morzelewski, A., Brodbeck, V., Borisov, S., Jahnke, K., Laufs, H., 2013. Large-scale brain functional modularity is reflected in slow electroencephalographic rhythms across the human non-rapid eye movement sleep cycle. *NeuroImage* 70, 327–339. doi:10.1016/j.neuroimage.2012.12.073
- Toppi, J., Babiloni, F., Vecchiato, G., De Vico Fallani, F., Mattia, D., Salinari, S., Milde, T., Leistriz, L., Witte, H., Astolfi, L., 2012a. Towards the time varying estimation of complex brain connectivity networks by means of a General Linear Kalman Filter approach. *Conf. Proc. IEEE Eng. Med. Biol. Soc.* 6192–6195. doi:10.1109/EMBC.2012.6347408
- Toppi, J., De Vico Fallani, F., Vecchiato, G., Maglione, A.G., Cincotti, F., Mattia, D., Salinari, S., Babiloni, F., Astolfi, L., 2012b. How the statistical validation of functional connectivity patterns can prevent erroneous definition of small-world properties of a brain connectivity network. *Comput. Math. Methods Med.* 130985. doi:10.1155/2012/130985
- Van Wijk, B.C.M., Stam, C.J., Daffertshofer, A., 2010. Comparing Brain Networks of Different Size and Connectivity Density Using Graph Theory. *PLoS One* 5. doi:10.1371/journal.pone.0013701
- Wascher, E., Rasch, B., Sanger, J., Hoffmann, S., Schneider, D., Rinkenauer, G., Heuer, H., Gutberlet, I., 2014. Frontal theta activity reflects distinct aspects of mental fatigue. *Biol. Psychol.* 96, 57–65. doi:10.1016/j.biopsycho.2013.11.010
- Watts, D.J., Strogatz, S.H., 1998. Collective dynamics of “small-world” networks. *Nature* 393, 440–442. doi:10.1038/30918

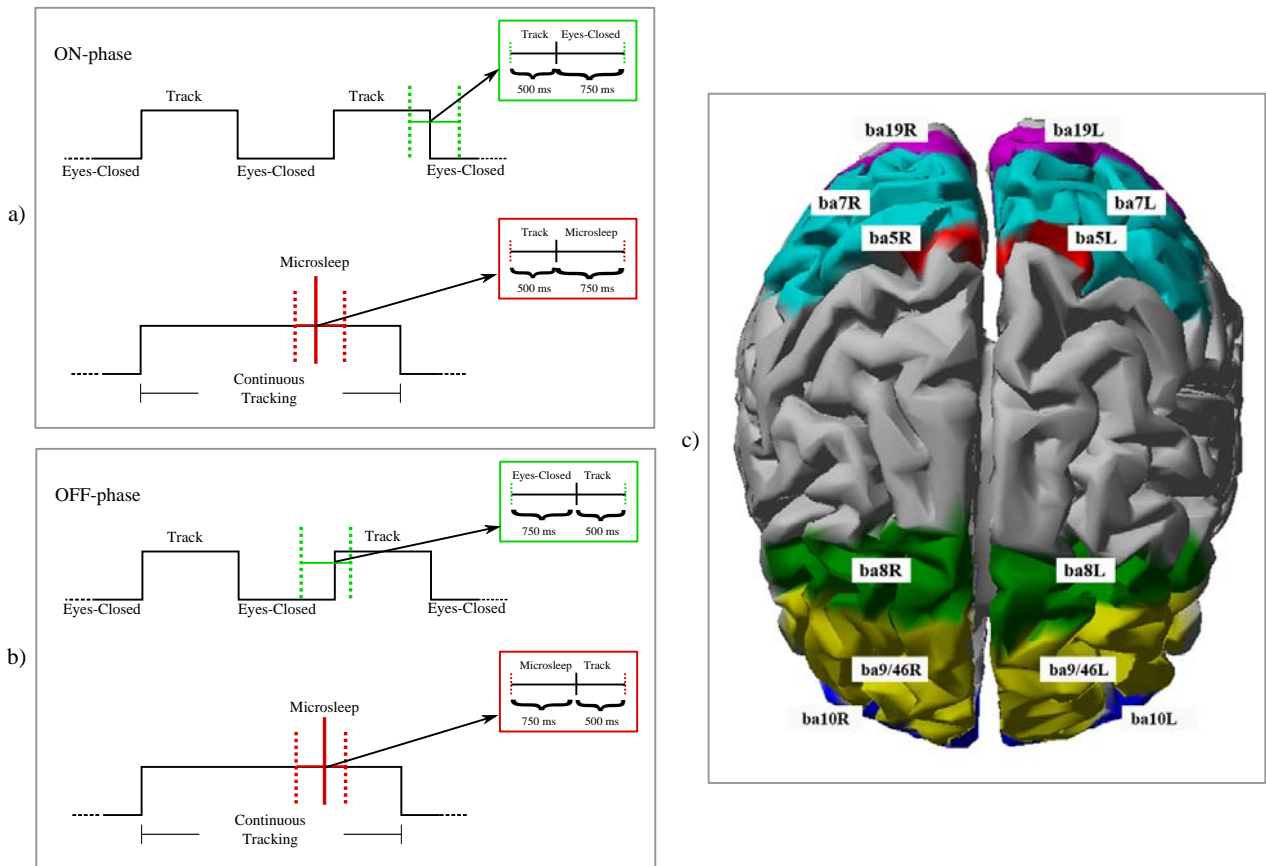


Fig. 1. a-b) Scheme of the two time windows (a: on-phase and b: off-phase) considered in the experiment for behavioral microsleeps events (red) and baseline (green) conditions. c) Graphical representation of the cortex model and regions of interest (ROIs). The model is the Colin template, MNI Institute. ROIs considered in study included the Brodmann Area (ba): 19L/R, 7L/R, 5L/R, 8L/R, 9/46L/R, 10L/R.

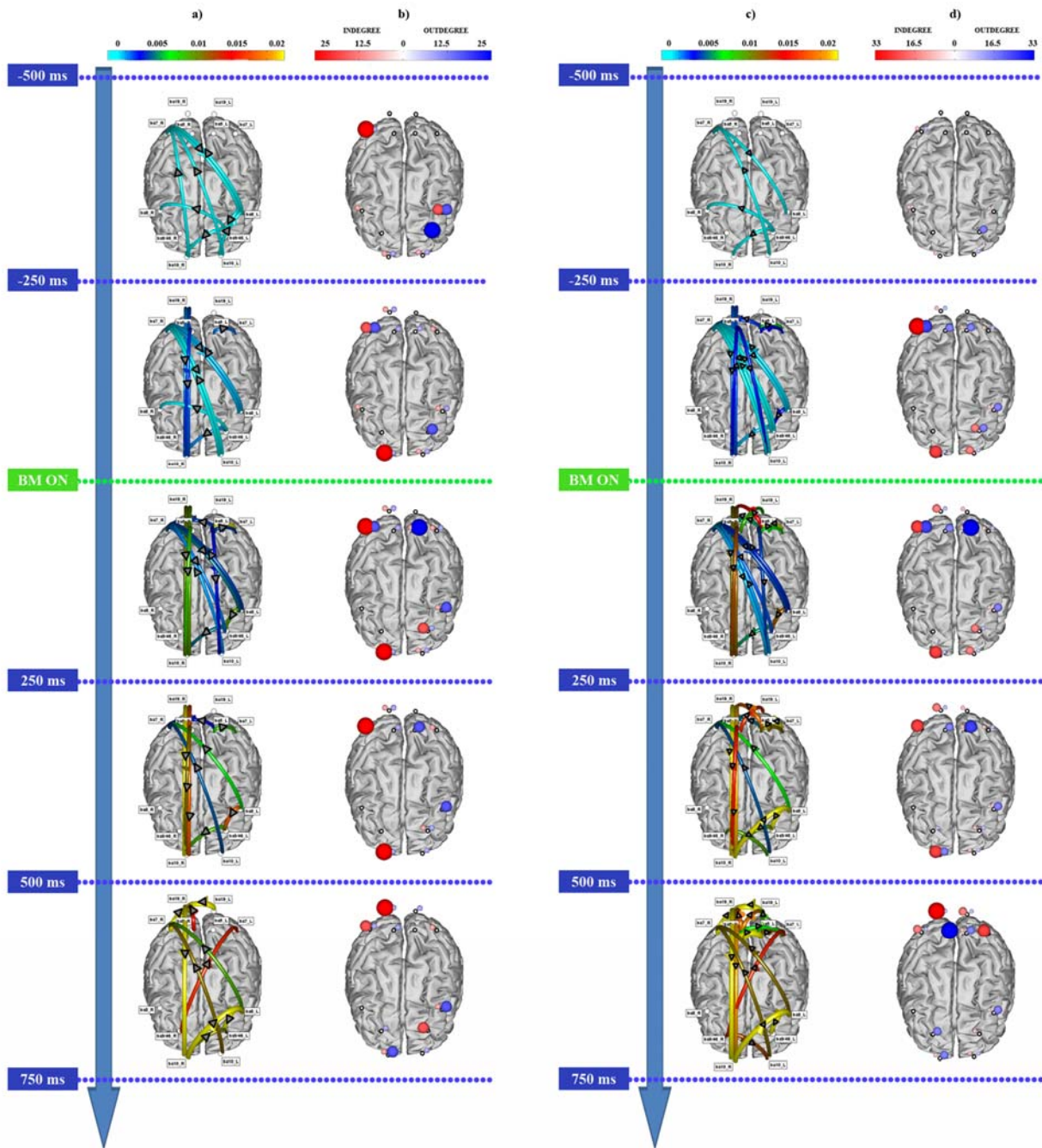


Fig. 2. a-c) Statistical group patterns of connectivity from N=10 subjects during the ON-phase in theta (panel a) and alpha (panel c) bands. Each network is related to a specific time interval defined according to the microsleeep onset: (-500 ; -250) ms, (-250 ; 0) ms, (0 ; 250) ms, (250 ; 500) ms, (500 ; 750) ms (BM – behavioral microsleeep). Connectivity patterns are represented on the realistic cortical model used for the analysis, which is seen from above, with the nose pointing to the bottom of the figure. Each connection between two cortical regions is represented by means of an arrow, whose colour and diameter code for the corresponding PDC value averaged in the population. The cortical regions of interest (ROIs) are highlighted with different colours (see Figure 1c for ROIs labels). b-d) Graphical representation of in-degree and out-degree indices computed for each ROI. Patterns are referred to the intervals defined in panels a and c. Circles colour and diameter code for the degree of the corresponding ROI (in-degree in red, out-degree in blue).

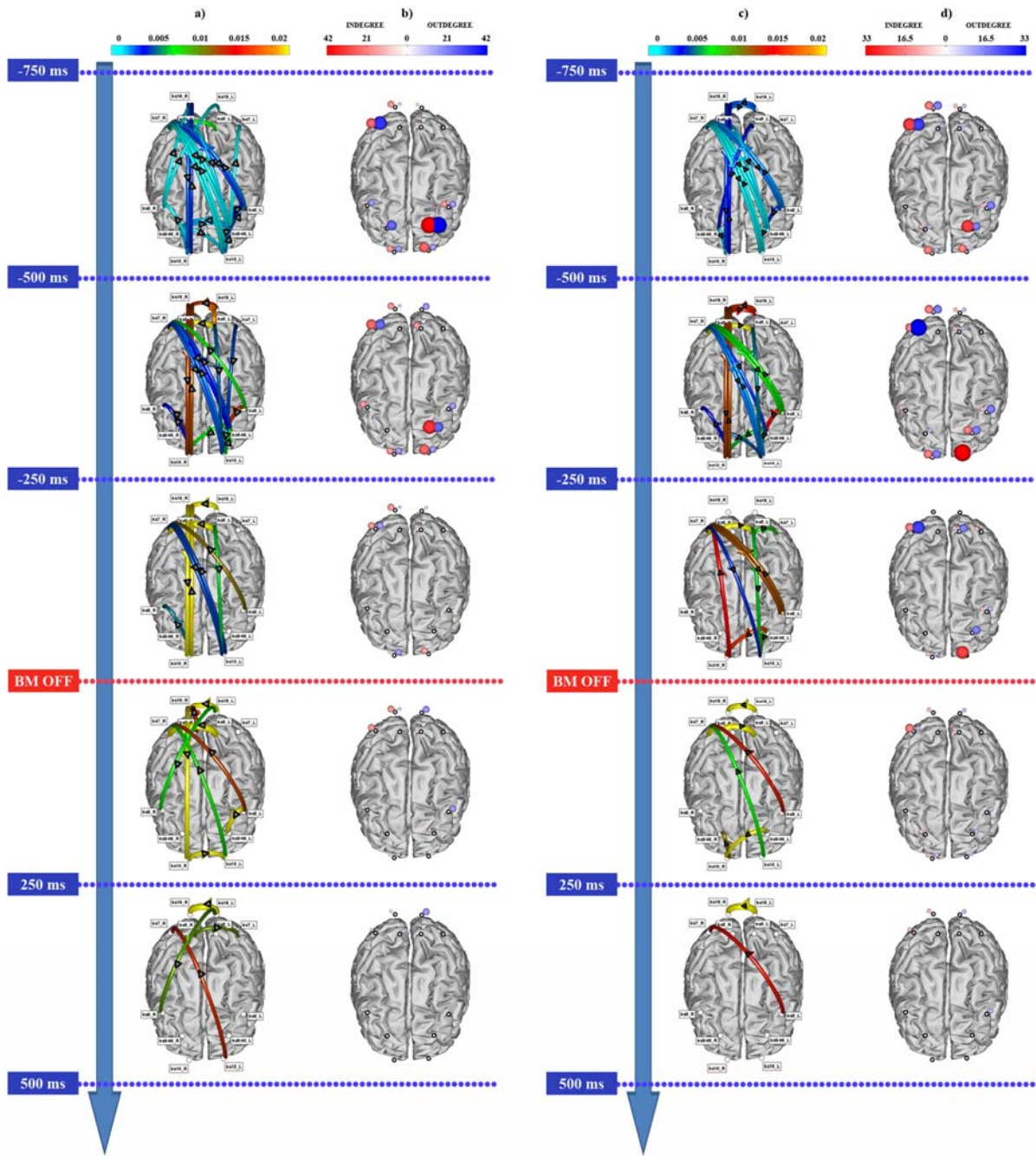


Fig. 3. a-c) Group statistical patterns of connectivity from N=10 subjects during the OFF-phase in theta (panel a) and alpha (panel c) bands. Each network is related to a specific time interval defined according to the microsleeep end: (-750 ; -500) ms, (-500 ; -250) ms, (-250 ; 0) ms, (0 ; 250) ms, (250 ; 500) ms (BM – behavioral microsleeep). Connectivity patterns are represented on the realistic cortical model used for the analysis, which is seen from above, with the nose pointing to the bottom of the figure. Each connection between two cortical regions is represented by means of an arrow whose colour and diameter code for the corresponding PDC value (averaged in the population, see colour bar). The cortical regions of interest (ROIs) are highlighted with different colours (see Fig.1c for ROIs labels). b-d) Graphical representation of in-degree and out-degree indices computed for each ROI. Patterns are referred to the intervals defined in panels a and c. Circles colour and diameter code for the degree of the corresponding ROI (in-degree in red, out-degree in blue).

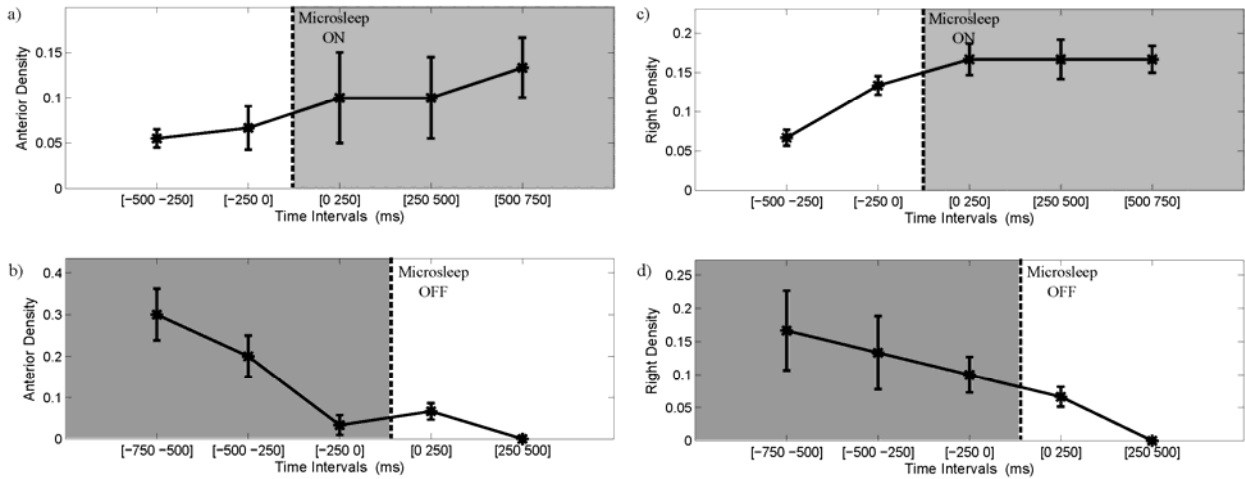


Fig. 4. Time-varying trend (mean \pm SD) of anterior areas density index (panels a and b) and right hemisphere density index (panels c and d) computed on the networks elicited in the theta band during the onset (panels a and c) and the end (panels b and d) of microsleeps events. Average values (N=10) computed for the five time intervals defined according to the onset and the end of microsleep (same intervals reported in Figs. 2,3). The microsleep time window is marked in grey. The periods preceding and following microsleeps are reported in white.

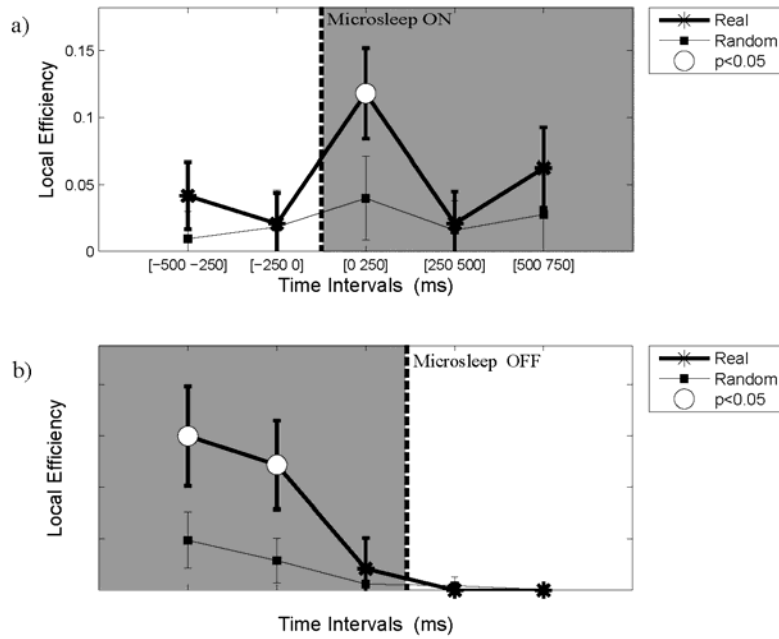


Fig. 5. Statistical comparison between local efficiency index (mean \pm SD) computed on microsleeps (star markers) and corresponding values computed for random networks (square markers) in the theta band, during the onset (panel a) and end (panel b) of microsleap events. Average values (N=10) computed for the five time intervals defined according to the onset and the end of microsleap (same intervals reported in Figs. 2,3). The microsleap time window is marked in grey. The periods preceding and following microsleap events are highlighted in white. The light grey circles indicate a significant difference between real and random networks ($p < 0.05$).

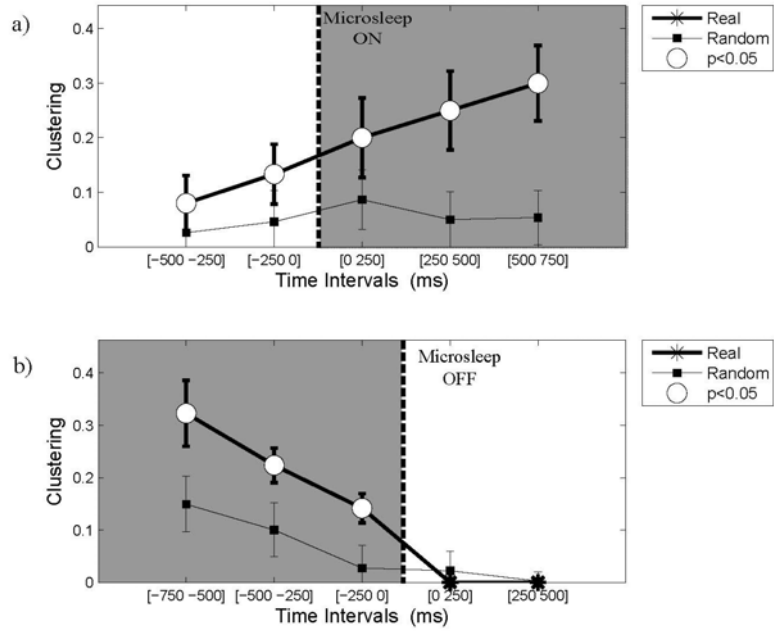


Fig. 6. Statistical comparison between the clustering index computed on microsleeps (mean \pm SD; star markers) and corresponding values computed for random networks (square markers) in the theta band, during the onset (panel a) and end (panel b) of microsleep events. Same representation of the previous figure.

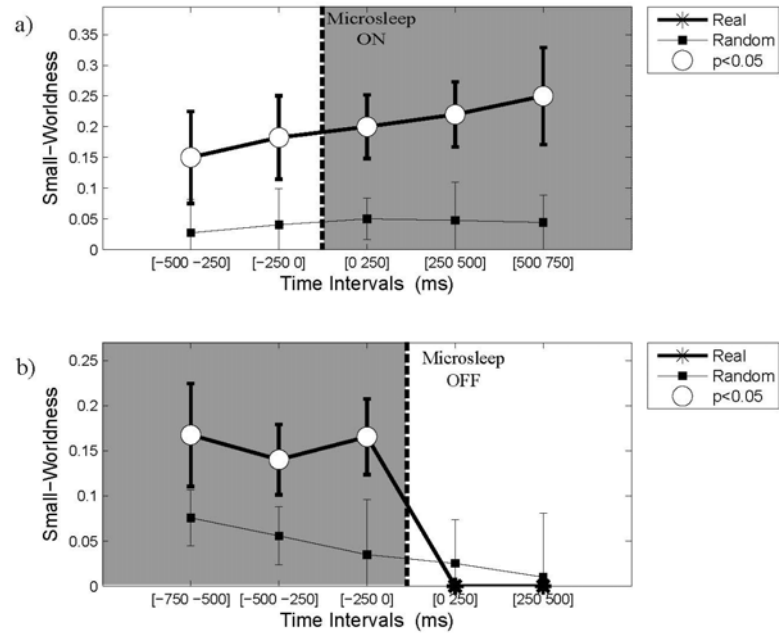


Fig. 7. Statistical comparison between Small-Worldness computed on microsleeps (mean \pm SD; star markers) and corresponding values computed for random networks (square markers) in the theta band, during the onset (panel a) and end (panel b) of microsleeper events. Same representation of the previous figures.